High-efficiency metal-free organic-dye-sensitized solar cells with hierarchical ZnO photoelectrode†

Hsin-Ming Cheng and Wen-Feng Hsieh*

Received 31st July 2009, Accepted 10th December 2009
First published as an Advance Article on the web 22nd January 2010
DOI: 10.1039/b915725e

Self-assembled ZnO secondary nanoparticles have been fabricated as an effective photoelectrode for dye-sensitized solar cells (DSCs). The hierarchical architecture, which manifested the significant light-scattering, can provide more photon harvesting. In addition, dye-molecule adsorption was sufficient due to enough internal surface area provided by the primary single nanocrystallites. Two indoline dyes, coded D149 and D205, were used as the sensitizers of ZnO DSCs with the optimal energy conversion efficiencies of 4.95% and 5.34%, respectively, under AM 1.5 full sunlight illumination (100 mW cm^{-2}). The enhancement of the open-circuit photovoltage (V_{oc}) and the short-circuit photocurrent density (J_{sc}) for D205-sensitized ZnO DSCs was ascribed to the effective suppression of electron recombination by extending the alkyl chain on the terminal rhodanine moiety from ethyl to octyl. Further evidence is obtained from the electrochemical impedance spectroscopy (EIS) which exhibits a longer electron lifetime for D205-sensitized ZnO DSC in comparison with the D149-sensitized one.

I. Introduction

Dye-sensitized solar cells (DSCs) with power conversion efficiencies exceeding 11% have been exhibited and remain one of the most promising candidates, as they possess advantages of being flexible, inexpensive, and easier to manufacture than other thin film solar cells.[1] In DSCs, the photoelectrodes are very important features, which include mesoporous wide-bandgap oxide semiconductor films with not only enormous internal surface area but also rapid electron injection from the lowest unoccupied molecular orbitals (LUMO) of dye molecules into the conduction band of the metal oxides. The highest solar-to-electric conversion efficiency of 11% has been achieved with films that consist of 20 nm TiO_2 nanocrystallites sensitized by ruthenium-based dyes.[1] ZnO is a versatile semiconductor having recently been reported as an alternative for DSCs because ZnO offers a large direct band gap of 3.37 eV, which is similar to TiO_2. In addition, ZnO has very high electron mobility for its relatively small electron effective mass as compared to TiO_2.[2] ZnO can also be tailored to various nanostructures, such as nanorods/nanowires,[3] nanotubes,[4] nanoflowers,[5] nanosheets,[6] tetrapod-like nanopowders,[7] and polydispersive ZnO aggregates.[8] The nanostructured ZnO can significantly enhance DSC performance by not only offering a large surface area for dye adsorption, but also direct transport pathways for photoexcited electrons. ZnO nanoarchitectures provide promising designs for improving the performance of the photoelectrodes in DSCs.

Utilizing sensitized dye with a high absorption coefficient is another key issue to improve the light harvesting of DSCs. Numerous metal-free organic dyes with high absorption coefficients have recently been reported to act as good sensitizers for TiO_2. Ruthenium complex dyes are not suitable for environmentally-friendly photovoltaic devices because they do not meet the low cost and mass production requirements needed for potentially wide applications. In particular, indoline dyes have been reported to show a highest power conversion efficiency of

Department of Photonics & Institute of Electro-Optical Engineering, National Chiao Tung University, Hsinchu, 300, Taiwan. E-mail: wfhsieh@mail.nctu.edu.tw; Fax: +886-3-5716631; Tel: +886-3-5712121 ext. 56316

† Electronic supplementary information (ESI) available: Micrographs; SEM and TEM images; X-ray diffraction profiles; wavelength distribution of incident monochromatic photon to current conversion efficiency spectra. See DOI: 10.1039/b915725e

Broader context

Dye-sensitized solar cells (DSCs) have been expected to be one of the most promising environmentally-friendly photovoltaic devices, as it possesses advantages of being flexible, low cost, and easier to manufacture than other brittle thin film solar cells. Design of nanostructured materials that provide sufficient light-harvesting capability and efficient electron transport becomes a key issue of these solar cells. ZnO has been intensely sought as a replacement for the TiO_2 photoelectrodes in DSCs because ZnO offers similar energy levels but higher electron mobility as compared with TiO_2. Furthermore, ZnO can be easily tailored to various nanostructures as compared to other metal oxides. Here we employ hierarchical ZnO secondary nanoparticles along with two different indoline dyes to construct a high molar extinction coefficient absorber. This concept provides effective light scattering within the photoelectrodes of DSCs, while retaining the desired specific surface area for dye-molecule adsorption. These novel hierarchical nanostructures provide a promising design for improving the performance of DSCs.

over 9.0% using volatile electrolytes[9] and an efficiency of 7.2% using nonvolatile ionic-liquid electrolytes[10] among organic dyes. The indoline dyes that exhibit remarkable performance as DSCs are relatively inexpensive due to the simple preparation procedures.[11] Recently, an indoline dye (D149) has also been utilized in ZnO nanosheets[6b] and tetrapod-like ZnO nanopowders,[7b] and achieved the DSC performances of 4.2% and 4.9%, respectively. Accordingly, a systematic study of the characterization in indoline-sensitized ZnO DSCs is important for both further dye molecular engineering and for photovoltaic application points of view.

In the present work, we reported that the photoanode films composed by self-assembled ZnO secondary nanoparticles provides effective light scattering within the photoelectrode films of DSCs while retaining the desired specific surface area for dye-molecule adsorption. Two indoline dyes, coded D149 and D205, were used as the sensitizers of DSCs. The effect of thickness on DSC performance will be discussed. The maximum energy conversion efficiencies of 4.95% and 5.34% were achieved on a 27 μm-thick ZnO photoelectrode film under AM 1.5 solar radiation for D149 and D205, respectively. The comparison of the electron transport property of ZnO photoelectrodes with different dyes will also be discussed based on the electrochemical impedance spectroscopy (EIS).

II. Experiments

Preparation of ZnO colloidals and screen-printing pastes

The ZnO colloidal solution was produced from zinc acetate dihydrate (99.5% $Zn(OAc)_2$, Riedel-deHaen) in diethylene glycol (99% DEG, TEDIA), similar to what we presented exhaustively before.[12] The as-synthesized solution was placed in a centrifuge operating at 8000 rpm for 30 min. After centrifugation, the precipitation of ZnO colloids was then redispersed in ethanol *via* high-speed stirring for 30 min. The excess DEG solvent was then removed by a second centrifugation. The ZnO paste for screen-printing was prepared typically by mixing resultant ZnO colloids, ethyl cellulose (EC) and terpineol (anhydrous, #86480, Fluka); the detailed procedure is as follows. EC (5–15 mPas, #46070, Fluka) and EC (30–70 mPas, #46080, Fluka) were individually dissolved in ethanol to yield 10 wt% solutions. Then 12 g EC (5–15) and 12 g EC (30–70) were added to a round bottomed rotavap flask containing 12 g ZnO colloids and 25 g terpineol. The mixture paste was dispersed in an ultrasonic bath and a rotary-evaporator (BUCHI V850) was used to remove the residual ethanol and water in the mixture. The final formulations of the ZnO pastes were made with a three-roll mill (EXAKT E50).

Cell fabrication and characterization

The DSCs consisted of many parts sandwiched together. The photoanodes were prepared by screen-printing the 0.28 cm^2 ZnO films with various thicknesses (18, 21, 27, and 32 μm) on fluorine-doped tin oxide (FTO) substrates (Nippon Sheet Glass Co. Ltd., 10 Ω/□, 3 mm thickness). The photoelectrodes were then gradually heated under an O_2 flow at 350 °C for 30 min to remove the organic materials in the paste. After cooling to room temperature, the ZnO photoelectrodes were immersed into a solution made of 0.3 mM D149 or D205 organic sensitizer (Chemicrea Inc.) with 0.6 mM chenodeoxycholic acid (CDCA, Sigma-Aldrich) in an acetonitrile/*tert*-butyl alcohol mixture (v/v = 1: 1) at 65 °C for 1 h. The counter electrodes were also made of NSG FTO glass on which the nanocrystalline Pt catalysts were deposited by decomposing from H_2PtCl_6 at 400 °C for 20 min. The internal space of the ZnO photoelectrodes and counter electrodes was separated by a 60 μm thick hot-melting spacer (Surlyn, DuPont), and was filled through a hole with volatile electrolytes which composed of 0.5 M 1,2-dimethyl-3-propylimidazolium iodide (PMII), 0.03 M I_2 (Sigma-Aldrich), and 0.5 M *tert*-butylpyridine (TBP, Sigma-Aldrich) in acetonitrile.

Instrumentation

The morphology and dimension of ZnO nanoparticles were characterized using a JEOL-6500 field emission scanning electron microscope (FESEM) operated at 5 kV. The advanced ZnO nanostructures were analyzed using JEOL JEM-2100F field emission transmission electron microscope (FETEM) operated at 200 kV. For photocurrent–voltage (J–V) characteristics and electrochemical impedance spectroscopy (EIS) measurements, a white light source (Yamashita Denso, YSS-100A) was used to give an irradiance of 100 mW cm^{-2} (the equivalent of one sun at AM 1.5) on the surface of the solar cells, and the data were collected by an electrochemical analyzer (Autolab, PGSTAT30). The light power was calibrated with a set of neutral density filters and detected by a silicon photodiode (BS-520, Bunko Keiki). The action spectra of the incident monochromatic photon to current conversion efficiency (IPCE) for solar cells were measured as a function of wavelength from 400 to 900 nm using a specially designed IPCE system (C^{-995}, PV-measurement Inc.) for DSCs. The optical absorbance was carried out with a Hitachi U-2800 UV-VIS spectrophotometer.

III. Results and discussion

Hierarchical packing of the secondary ZnO nanoparticles was formed in the condensation reactions of the sol–gel process, which was modified from the previous reports.[13] The spherical shape of the secondary ZnO nanoparticles was recognized as an agglomeration of many primary single crystallites ranging from 6 to 12 nm, as shown in Fig. 1(a) and 1(b). The similar ZnO architectures have been elucidated as random lasers formed in the cavities by multiple scattering between ZnO primary particles.[14] The laser action could emerge for the efficient amplification along the closed loop light-scattering paths within a secondary ZnO nanoparticle. Recently, Cao *et al.*[8] demonstrated that the aggregation of ZnO nanocrystallites performed was an effective approach to generate light scattering within the photoelectrode film of DSCs without using any other scattering layers. In addition, dye-molecule adsorption was sufficient due to enough internal surface area provided by the primary nanocrystallites and a maximum energy conversion efficiency of 5.4% has been achieved with utilization of ruthenium complex *cis*-$[RuL_2(NCS)_2]$ (L = 4,4′-dicarboxy-2,2′-bipyridine), N3 dye. Herein, the broad distribution of secondary nanoparticle sizes, with diameters in the range of 200–500 nm, was controlled to provide the wide range absorption of visible sun light within the

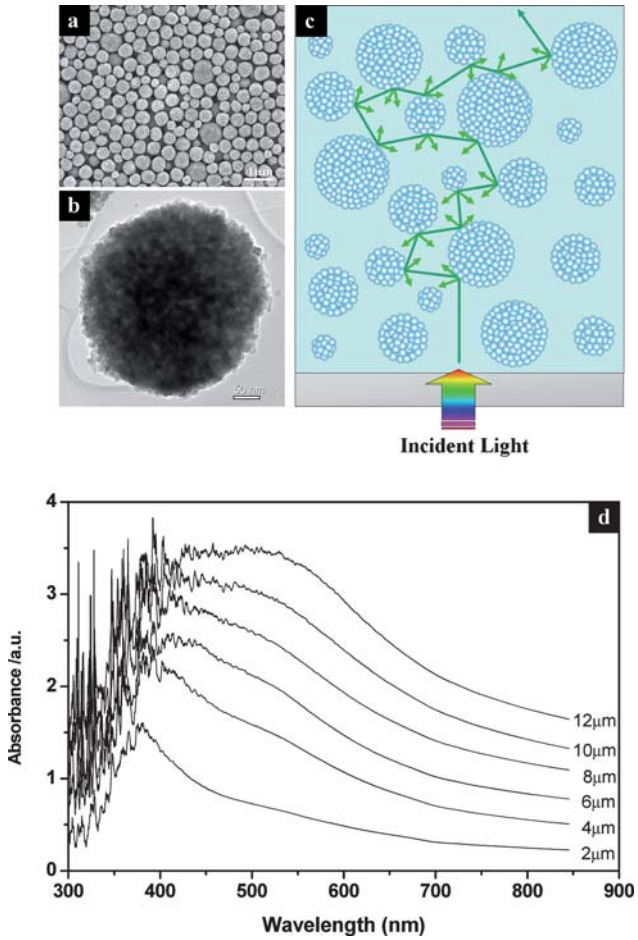

Fig. 1 (a and b) The FESEM and TEM images for the self-assembled ZnO secondary nanoparticles, respectively. (c) The schematic multiple scattering of light within the hierarchical ZnO photoelectrode composed by self-assembled ZnO secondary nanoparticles. (d) The corresponding optical absorption spectra of ZnO photoelectrodes with various film thicknesses, from 2μm to 12 μm.

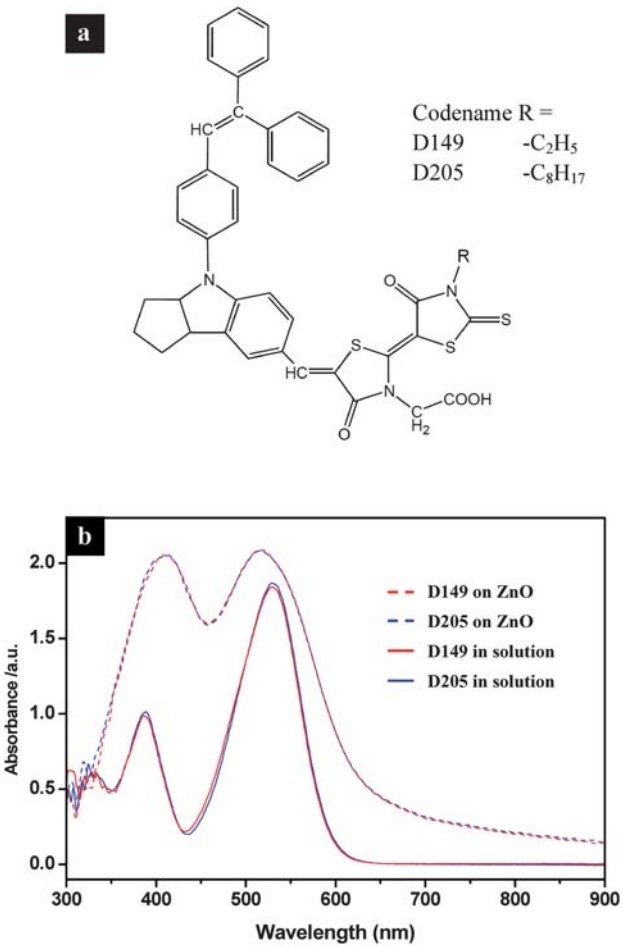

Fig. 2 (a) Molecular structures of indoline D149 and D205 dyes. (b) Absorption spectra of D149 and D205 dyes in *tert*-butyl alcohol/acetonitrile (1/1) solution and on the 4 μm-thick ZnO photoelectrodes, respectively.

preferable packing of the ZnO photoelectrode. Fig. 1(c) shows a schematic of the multiple scattering of light within the hierarchical ZnO photoelectrode, and that therefore the light-traveling distance can be significantly prolonged. Fig. 1(d) also shows the corresponding optical absorption spectra of ZnO photoelectrodes with various film thicknesses. The absorption peak at 375 nm, which could be particularly identifiable from the 2 μm film, mainly results from the intrinsic exciton absorption of ZnO. However, the absorption at wavelengths of around 400–650 nm is enhanced dramatically with increasing the thickness of the ZnO photoelectrodes from 2 μm to 12 μm. The ZnO films with thicknesses above 10 μm provide light localization through significant light scattering from the highly disordered structure. The results explain the light-scattering capability of the films with different thicknesses and the formation of optical confinement through the aggregated ZnO films, which could provide more photon absorption in the visible region by the dye molecules.

The molecular structures of the indoline-based organic dyes employed in this study are depicted in Fig. 2(a). The double rhodanic acid was used as an anchor moiety for both D149 and D205. The D205 sensitizer was designed by introducing an octyl substitute onto the terminal rhodanine ring to replace the ethyl group of D149. Fig. 2(b) shows the light absorption spectra of D149 and D205 in *tert*-butyl alcohol/acetonitrile (1/1) and on the 4 μm-thick ZnO photoelectrodes, respectively. The absorption spectra of D149 and D205 in solution are almost identical, revealing that the indoline dye D205 has almost the same molecular coefficient value (68700 M^{-1} cm^{-1} at 526 nm) as D149 in *tert*-butyl alcohol/acetonitrile (1/1).[11b] The absorption spectra of D149 and D205 on the ZnO photoelectrodes have the broadened peaks and a blue-shift of the main absorption peak centered around 516 nm that indicate these indoline dyes have a moderate interaction between dye molecules on the ZnO surface. The red-shift of absorption peaks at low wavelength for indoline dyes on ZnO could be related to the influence of the thickness effect on the photoelectrode (see Fig. 1(d)). The blue-shift, from 530 nm (indoline dyes in the solution) to 516 nm (indoline dyes on ZnO films), of the main absorption peak could be addressed as a hypsochromic shift due to H-aggregation. The observation is different from the previous reports concerning the indoline dye on TiO_2.[9b, 10,11] The origin is mainly attributed to the formation of a bidentate complex between the carboxylate and the polar zinc oxide surface.[15] However, further investigation on

the interactions of dye aggregation are presently being analyzed to lead to better understanding of the dynamics of DSCs.

In order to improve the DSC performance, optimization of the thickness of the ZnO photoelectrode is necessary because the photovoltaic characteristics exhibit significant variation depending on the thickness. Fig. 3 shows the variations in the photovoltaic characteristics of DSCs depending on the thickness of the indoline dye-sensitized hierarchical ZnO photoelectrode. The open-circuit photovoltage (V_{oc}) decreased linearly with the increase in ZnO film thickness (Fig. 3a). Increasing the thickness leads to increasing the non-excited area, which lowers V_{oc} further after averaging the electron density in the non-excited area. On the contrary, the short-circuit photocurrent density (J_{sc}) for DSCs using both indoline dyes increases monotonically with increasing ZnO film thickness (Fig. 3b), as a result of enlarged dye loading. In addition, V_{oc} and J_{sc} for D205-sensitized ZnO DSCs are higher than D149-sensitized ones. This observation can be ascribed to the effective suppression of electron recombination between I_3^- and electrons injected in the photoelectrodes by extending the alkyl chain on the terminal rhodanine moiety from ethyl to octyl.[16] Further examination will be later described *via* the electron transport analysis. The fill factor (FF) for D205-sensitized ZnO DSCs is slightly lower than that of D149-sensitized ZnO DSCs, which is rationalized in terms of the series resistance of the DSC: the higher J_{sc} values end up with lower FF values. Although V_{oc} decreases with the ZnO film thickness, this loss of V_{oc} is compensated by a gain in J_{sc} and consequently the maximum energy conversion efficiencies (η) of 4.95% and 5.34% were achieved for D149- and D205-sensitized ZnO DSCs, respectively, with a 27 μm-thick ZnO photoelectrode film under AM 1.5 solar radiation. It should be noted that the influence of the thickness effect on the performance of DSCs utilizing secondary ZnO nanoparticles is relatively small in comparison with utilizing tetrapod-like ZnO nanoparticles in our previous report.[7b] A possible explanation for this is ascribed to the sufficient light-harvesting capability of these hierarchical ZnO architectures when even quite thin photoelectrodes are applied.

Fig. 4(a) shows the detailed comparison of photocurrent–voltage (J–V) characteristics for solar cells constructed using 27 μm-thick ZnO photoelectrode films and these two different indoline dyes under AM 1.5 full sunlight illumination (100 mW cm^{-2}) and in the dark. For D205 uptake, the spectrum reveals V_{oc} = 653 mV, J_{sc} = 12.17 mA cm^{-2}, FF, = 0.67, and η = 5.34%. For comparison, the spectrum of D149 uptake reveals V_{oc} = 641 mV, J_{sc} = 10.94 mA cm^{-2}, FF = 0.7, and η = 4.95%. The curves of dark current also indicated that D205-sensitized ZnO DSC has a slightly lower onset potential for the reduction of I_3^- than D149-sensitized ZnO DSC. The lower dark current could also be rationalized in terms of a negative shift in the conduction band edge of ZnO caused by the adsorption of D205 dye. Fig. 4(b) displays the wavelength distribution of the incident monochromatic photon to current conversion efficiency (IPCE) spectra of DSCs. Because of the UV cut-off effect caused by the thick glass substrate, the spectra at under 400 nm are deteriorated. However, the photocurrents at the peak at approximately 367 nm can still be detected and is due to direct light harvesting

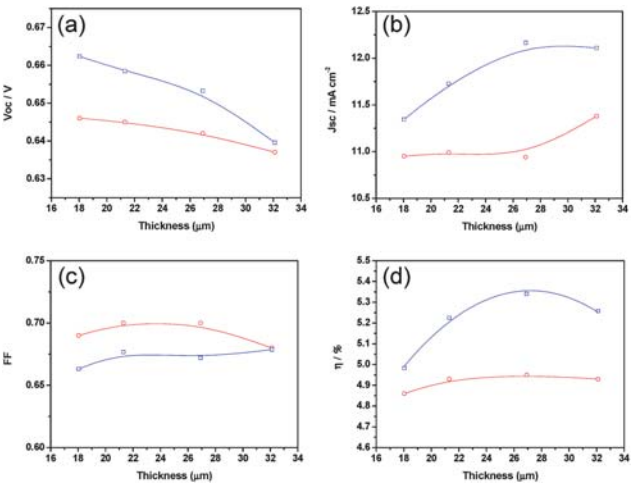

Fig. 3 Relationship between photovoltaic characteristics and photoelectrode thickness of ZnO DSCs. Red circles and blue squares represent D149- and D205-sensitized DSCs, respectively. (a) Open-circuit photovoltage, V_{oc}; (b) Short-circuit photocurrent density, J_{sc}; (c) Fill factor, FF; and (d) photopower energy conversion efficiency, η. The solid lines are plotted to guide the eyes.

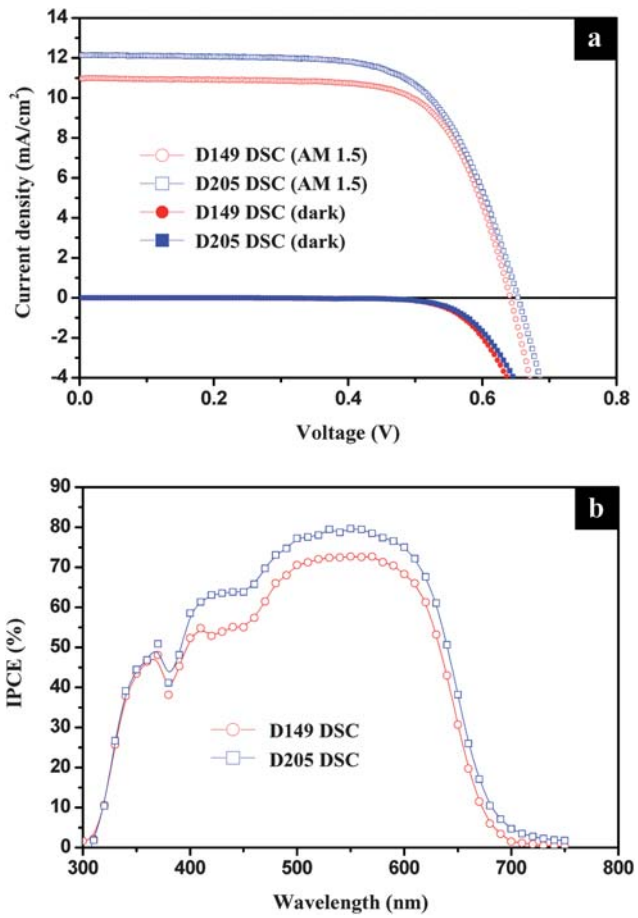

Fig. 4 Photovoltaic characteristics of DSCs with 27 μm-thick ZnO photoelectrodes and two different indoline dyes: (a) photocurrent–voltage (J–V) curves for D149- and D205-sensitized DSCs with AM 1.5 illumination and in the dark, respectively. (b) photocurrent action spectra of D149- and D205-sensitized DSCs, respectively.

by the ZnO semiconductor. The IPCE obtained for the D205-sensitized ZnO DSC is higher than that of the D149-sensitized one in the visible-wavelength (400–700 nm) region. The evidence of the improvement in the IPCE further confirms the higher J_{sc} for the D205-sensitized ZnO DSC as compared with the D149-sensitized ZnO DSC. The superior performance for D205 dye uptake is attributed to extending the length of the alkyl chain on the indoline sensitizer. In general, the current density for DSCs is determined by the initial number of photogenerated carriers, the electron injection efficiency from dye molecules to semiconductor, and the recombination rate between the injected electrons and oxidized dye or redox species in the electrolyte. Based on the assumption of the same injection efficiency and dye loading for the given ZnO DSCs systems, it is reasonable that the photocurrent density may be directly affected by the variation in the electron recombination rate. The amphiphilic nature of D205 may assist the formation of a self-assembled dye monolayer that prevents the recapture of the photoinjected electrons by the triiodide ions within the electrolyte, consequently resulting in a higher V_{oc} and J_{sc}.[10]

The effects of the different dyes on the electron transport of the interfaces in the DSCs can be further investigated with aid of the electrochemical impedance spectroscopy (EIS) study. Adequate physical models and equivalent circuits have been proposed and widely applied to analyze the electron transport in photoelectrodes and recombination between the photoelectrode and electrolyte interface in the DSC.[17] The Nyquist plots of the impedance data for D149-, and D205-sensitized ZnO DSCs were performed by applying a 10 mV ac signal over the frequency range of 10^{-2}–10^{5} Hz under illumination at the applied bias of V_{oc}, as shown in Fig. 5. The Nyquist plots in Fig. 5(a) show the radius of the middle semicircle, which belongs to D205-sensitized ZnO DSCs, is larger than D149-sensitized ZnO DSCs, indicating that the electron recombination resistance is enlarged from D149 to D205. In addition, from the Bode phase plot in Fig. 5(b), the mid-frequency peak apparently shifts to a lower frequency, corresponding to an increase of the electron lifetime (τ) for D205-sensitized ZnO DSCs. The electron lifetime can also be extracted from the angular frequency (ω_{min}) at the mid-frequency peak in the Bode phase plot using $\tau = 1/\omega_{min}$, and was derived to be 12.8 and 15.3 ms for D149- and D205-sensitized ZnO DSCs, respectively. The increase in electron lifetime supports more effective suppression of the back reaction of the injected electrons with the I_3^- in the electrolyte by means of extending the length of alkyl chain on the indoline sensitizer, which leads to the improvement in the photocurrent and photovoltage and to the substantial enhancement of the device efficiency. The low- and high-frequency peaks observed in the Bode plots correspond to triiodide diffusion in the electrolyte and charge transfer at the counter electrode, respectively. There are no significant changes of low- and high-frequency peaks observed in the Bode plots implying that no unexpected reaction had occurred within the electrolyte and the counter electrode through the octyl substitution of indoline dye.

Comparative experiments reported on metal-free indoline dyes emphasize the importance of improving the photovoltaic performance by suitable molecular engineering. The unambiguous enhancement of photopower-conversion efficiency was achieved by extending the length of alkyl chain on the indoline sensitizer with the hierarchical photoelectrode composed by aggregated ZnO secondary nanoparticles. Although the efficiency of ZnO DSC cannot compete with TiO_2 DSC systems presently, we hope these investigations could shed light on the development of organic sensitizers and can be used in the ZnO nanostructure optimization for the proposed solar cell applications.

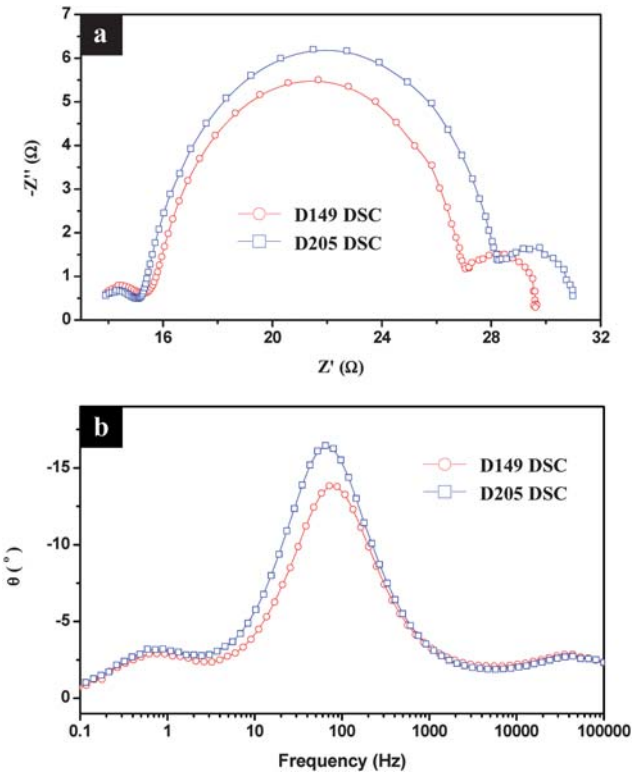

Fig. 5 Impedance spectra: (a) Nyquist plots, and (b) Bode phase plots of D149- and D205-sensitized DSCs performed under illumination at the applied bias of V_{oc}.

IV. Conclusion

In summary, self-assembled ZnO secondary nanoparticles have been demonstrated as an effective photoelectrode within DSCs which retain the desired specific surface area for dye-molecule adsorption and sufficient light-harvesting from prolonged light traveling. D149 and D205 indoline dyes were used as the sensitizers of ZnO DSCs. The optimized energy conversion efficiencies of 4.95% and 5.34% were achieved on 27 μm-thick ZnO photoelectrode films under AM 1.5 solar radiation, for D149 and D205, respectively. The enhancement of V_{oc} and J_{sc} for D205-sensitized ZnO DSCs is ascribed to the effective suppression of electron recombination by extending the alkyl chain on the terminal rhodanine moiety from ethyl to octyl. The results of the comparison of the electron transport property is further confirmed by the electrochemical impedance spectroscopy (EIS) that demonstrates electron lifetimes of 12.8 and 15.3 ms for D149- and D205-sensitized ZnO DSCs, respectively. Thus, the hybrid system of hierarchical ZnO architecture and metal-free indoline sensitizer represents an alternative candidate with regard to high-performance DSCs.

Acknowledgements

Authors acknowledge PVTC/ITRI for facilities support and financial support from the National Science Council (NSC) of Taiwan (Project No. NSC-96-2628-M-009-001-MY3) and from MCL/ITRI (Project No. 8301XSY4X1).

Notes and references

1 (*a*) M. Grätzel, *Inorg. Chem.*, 2005, **44**, 6841; (*b*) M. K. Nazeeruddin, F. DeAngelis, S. Fantacci, A. Selloni, G. Viscardi, P. Liska, S. Ito, B. Takeru and M. Grätzel, *J. Am. Chem. Soc.*, 2005, **127**, 16835; (*c*) L. Moreira Gonçalves, V. de Zea Bermudez, H. Aguilar Ribeiro and A. M. Mendes, *Energy Environ. Sci.*, 2008, **1**, 655.

2 (*a*) G. Oskam, Z. S. Hu, R. L. Penn, N. Pesika and P. C. Searson, *Phys. Rev. E: Stat., Nonlinear, Soft Matter Phys.*, 2002, **66**, 011403; (*b*) Ü. Özgür, Y. I. Alivov, C. Liu, A. Teke, M. A. Reshchikov, S. Doğan, V. Avrutin, S. J. Cho and H. Morkoç, *J. Appl. Phys.*, 2005, **98**, 041301; (*c*) S. J. Pearton, D. P. Norton, K. Ip, Y. W. Heo and T. Steiner, *Prog. Mater. Sci.*, 2005, **50**, 293.

3 (*a*) M. Law, L. E. Greene, J. C. Johnson, R. Saykally and P. D. Yang, *Nat. Mater.*, 2005, **4**, 455; (*b*) J. B. Baxter and E. S. Aydil, *Appl. Phys. Lett.*, 2005, **86**, 053114; (*c*) A. Du Pasquier, H. Chen and Y. Lu, *Appl. Phys. Lett.*, 2006, **89**, 253513; (*d*) H. M. Cheng, W. H. Chiu, C. H. Lee, S. Y. Tsai and W. F. Hsieh, *J. Phys. Chem. C*, 2008, **112**, 16359; (*e*) I. Gonzalez-Valls and M. Lira-Cantu, *Energy Environ. Sci.*, 2009, **2**, 19.

4 (*a*) A. B. F. Martinson, J. W. Elam, J. T. Hupp and M. J. Pellin, *Nano Lett.*, 2007, **7**, 2183; (*b*) A. B. F. Martinson, M. S. Góes, F. Fabregat-Santiago, J. Bisquert, M. J. Pellin and J. T. Hupp, *J. Phys. Chem. A*, 2009, **113**, 4015.

5 C. Y. Jiang, X. W. Sun, G. Q. Lo, D. L. Kwong and J. X. Wang, *Appl. Phys. Lett.*, 2007, **90**, 263501.

6 (*a*) E. Hosono, S. Fujihara, I. Honma and H. Zhou, *Adv. Mater.*, 2005, **17**, 2091; (*b*) E. Hosono, Y. Mitsui and H. Zhou, *Dalton Trans.*, 2008, 5439.

7 (*a*) Y. F. Hsu, Y. Y. Xi, C. T. Yip, A. B. Djurišić and W. C. Chan, *J. Appl. Phys.*, 2008, **103**, 083114; (*b*) W. H. Chiu, C. H. Lee, H. M. Cheng, H. F. Lin, S. C. Liao, J. M. Wu and W. F. Hsieh, *Energy Environ. Sci.*, 2009, **2**, 694; (*c*) W. Chen, H. Zhang, I. M. Hsing and S. Yang, *Electrochem. Commun.*, 2009, **11**, 1057.

8 (*a*) T. P. Chou, Q. Zhang, G. E. Fryxell and G. Cao, *Adv. Mater.*, 2007, **19**, 2588; (*b*) Q. Zhang, T. P. Chou, B. Russo, S. A. Jenekhe and G. Cao, *Angew. Chem., Int. Ed.*, 2008, **47**, 2402.

9 (*a*) S. Ito, S. M. Zakeeruddin, R. Humphry-Baker, P. Liska, R. Charvet, P. Comte, M. K. Nazeeruddin, P. Péchy, M. Takata, H. Miura, S. Uchida and M. Grätzel, *Adv. Mater.*, 2006, **18**, 1202; (*b*) S. Ito, H. Miura, S. Uchida, M. Takata, K. Sumioka, P. Liska, P. Comte, P. Péchy and M. Grätzel, *Chem. Commun.*, 2008, 5194.

10 D. Kuang, S. Uchida, R. Humphry-Baker, S. M. Zakeeruddin and M. Grätzel, *Angew. Chem., Int. Ed.*, 2008, **47**, 1923.

11 (*a*) T. Horiuchi, H. Miura and S. Uchida, *Chem. Commun.*, 2003, 3036; (*b*) T. Horiuchi, H. Miura, K. Sumioka and S. Uchida, *J. Am. Chem. Soc.*, 2004, **126**, 12218.

12 (*a*) H. M. Cheng, H. C. Hsu, S. L. Chen, W. T. Wu, C. C. Kao, L. J. Lin and W. F. Hsieh, *J. Cryst. Growth*, 2005, **277**, 192; (*b*) H. M. Cheng, K. F. Lin, H. C. Hsu, C. J. Lin, L. J. Lin and W. F. Hsieh, *J. Phys. Chem. B*, 2005, **109**, 18385.

13 (*a*) D. Jezequel, J. Guenot, N. Jouini and F. Fievet, *Mater. Sci. Forum*, 1994, **152–153**, 339; (*b*) E. W. Seelig, B. Tang, A. Yamilov, H. Cao and R. P. H. Chang, *Mater. Chem. Phys.*, 2003, **80**, 257.

14 H. Cao, Y. G. Zhao, S. T. Ho, E. W. Seelig, Q. H. Wang and R. P. H. Chang, *Phys. Rev. Lett.*, 1999, **82**, 2278.

15 T. Dentani, Y. Kubota, K. Funabiki, J. Jin, T. Yoshida, H. Minoura, H. Miura and M. Matsui, *New J. Chem.*, 2009, **33**, 93.

16 J. E. Kroeze, N. Hirata, S. Koops, Md. K. Nazeeruddin, L. Schmidt-Mende, M. Grätzel and J. R. Durrant, *J. Am. Chem. Soc.*, 2006, **128**, 16376.

17 (*a*) J. Bisquert, *J. Phys. Chem. B*, 2002, **106**, 325; (*b*) J. Bisquert, *Phys. Chem. Chem. Phys.*, 2003, **5**, 5360; (*c*) J. Bisquert, A. Zaban, M. Greenshtein and I. Mora-Seró, *J. Am. Chem. Soc.*, 2004, **126**, 13550; (*d*) Q. Wang, J. E. Moser and M. Grätzel, *J. Phys. Chem. B*, 2005, **109**, 14945; (*e*) Q. Wang, S. Ito, M. Grätzel, F. Fabregat-Santiago, I. Mora-Seró, J. Bisquert, T. Bessho and H. Imai, *J. Phys. Chem. B*, 2006, **110**, 25210; (*f*) M. Adachi, M. Sakamoto, J. Jiu, Y. Ogata and S. Isoda, *J. Phys. Chem. B*, 2006, **110**, 13872.